Neurobiology of Disease 152 (2021) 105292

Contents lists available at ScienceDirect

Neurobiology of Disease

journal homepage: www.elsevier.com/locate/ynbdi

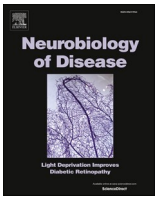

Bacterial sepsis increases hippocampal fibrillar amyloid plaque load and neuroinflammation in a mouse model of Alzheimer's disease

Jacob M. Basak [a,1], Aura Ferreiro [b], Lucy S. Cohen [c,d], Patrick W. Sheehan [c,d], Collin J. Nadarajah [c,d], Michael F. Kanan [c,d], Kimberley V. Sukhum [b,e], Gautam Dantas [b,e,f,g], Erik S. Musiek [c,d,h,*]

[a] Department of Anesthesiology, Washington University School of Medicine in St. Louis, St. Louis, MO 63110, USA
[b] Edison Family Center for Genome Sciences & Systems Biology, Washington University School of Medicine in St. Louis, St. Louis, MO 63110, USA
[c] Department of Neurology, Washington University School of Medicine in St. Louis, St. Louis, MO 63110, USA
[d] Hope Center for Neurological Disorders, Washington University School of Medicine in St. Louis, St. Louis, MO 63110, USA
[e] Department of Pathology and Immunology, Washington University School of Medicine in St. Louis, St. Louis, MO 63110, USA
[f] Department of Molecular Microbiology, Washington University School of Medicine in St. Louis, St. Louis, MO 63110, USA
[g] Department of Biomedical Engineering, Washington University in St. Louis, St. Louis, MO 63130, USA
[h] Charles F. and Joanne Knight Alzheimer's Disease Research Center, Washington University School of Medicine in St. Louis, St. Louis, MO 63110, USA

ARTICLE INFO

Keywords:
Sepsis
Alzheimer's disease
Amyloid-beta
Neuroinflammation
Complement
Microbiome

ABSTRACT

Background: Sepsis, a leading cause for intensive care unit admissions, causes both an acute encephalopathy and chronic brain dysfunction in survivors. A history of sepsis is also a risk factor for future development of dementia symptoms. Similar neuropathologic changes are associated with the cognitive decline of sepsis and Alzheimer's disease (AD), including neuroinflammation, neuronal death, and synaptic loss. Amyloid plaque pathology is the earliest pathological hallmark of AD, appearing 10 to 20 years prior to cognitive decline, and is present in 30% of people over 65. As sepsis is also more common in older adults, we hypothesized that sepsis might exacerbate amyloid plaque deposition and plaque-related injury, promoting the progression of AD-related pathology.
Methods: We evaluated whether the brain's response to sepsis modulates AD-related neurodegenerative changes by driving amyloid deposition and neuroinflammation in mice. We induced polymicrobial sepsis by cecal ligation and puncture (CLP) in APP/PS1–21 mice, a model of AD-related β-amyloidosis. We performed CLP or sham surgery at plaque onset (2 months of age) and examined pathology 2 months after CLP in surviving mice.
Results: Sepsis significantly increased fibrillar amyloid plaque formation in the hippocampus of APP/PS1–21 mice. Sepsis enhanced plaque-related astrocyte activation and complement *C4b* gene expression in the brain, both of which may play a role in modulating amyloid formation. CLP also caused large scale changes in the gut microbiome of APP/PS1 mice, which have been associated with a pro-amyloidogenic and neuroinflammatory state.
Conclusions: Our results suggest that experimental sepsis can exacerbate amyloid plaque deposition and plaque-related inflammation, providing a potential mechanism for increased dementia in older sepsis survivors.

List of Abbreviations

Aβ	amyloid-beta peptide
AD	Alzheimer's disease
APP	amyloid precursor protein
CLP	colonic ligation and perforation
LPS	lipopolysaccharide
PS1	presenilin-1
qPCR	quantitative polymerase chain reaction

(*continued on next column*)

(*continued*)

* Corresponding author at: Department of Neurology, Washington University School of Medicine, 440 South Euclid Avenue, Box 8111, St. Louis, MO 63110, USA.
E-mail address: musieke@wustl.edu (E.S. Musiek).
[1] Department of Anesthesiology, University of Colorado Denver, Anschutz Medical Campus, 12,800 E. 19th Ave, Aurora, CO 80045, USA.

https://doi.org/10.1016/j.nbd.2021.105292
Received 15 July 2020; Received in revised form 6 November 2020; Accepted 3 February 2021
Available online 5 February 2021

1. Background

Patients who survive an acute critical illness in the intensive care unit (ICU) are at increased risk for long-term cognitive dysfunction (Pandharipande et al., 2013). These cognitive changes often limit return of the individual to their daily activities, and place a significant burden on caregivers and society. One of the leading causes of critical illness in most intensive care units is sepsis and its associated multiorgan inflammatory response (Hotchkiss et al., 2016). Sepsis is associated with an acute and rapid change in cognition and memory, a condition known as septic encephalopathy (Gofton and Young, 2012). With improvements in mortality outcomes from sepsis along with the ongoing surveillance of survivors, it has become apparent that these cognitive changes may persist for years in those who recover from their illness (Iwashyna et al., 2010; Iwashyna et al., 2012; Semmler et al., 2013). These long-term changes contribute significantly to ongoing disability among these individuals and may potentially place them at increased risk for further neurological sequelae in the future, such as the development of dementia or neurodegenerative diseases (Widmann and Heneka, 2014).

The specific mechanisms underlying the neurologic changes with sepsis are challenging to fully elucidate given the complexity of the condition. In the acute setting, multiple pathological processes likely play a role in causing neuronal dysfunction. Animal models of systemic sepsis, including intraperitoneal lipopolysaccharide (LPS) administration and cecal ligation and puncture (CLP), demonstrate an increase in pro-inflammatory cytokines and chemokines in the brain (Erickson and Banks, 2011; Gasparotto et al., 2018; Semmler et al., 2008; Skelly et al., 2013; Zhao et al., 2019). The migration of neutrophils and monocytes from the periphery along with the local activation of microglia also contribute to the robust neuroinflammatory response (Aguilar-Valles et al., 2014; Henry et al., 2009; Michels et al., 2015). The presence of systemic-derived cells and inflammatory mediators suggest a breakdown in the blood-brain barrier, which could also lead to localized edema in the brain (Banks et al., 2015; Bozza et al., 2010; Hofer et al., 2008). Finally, the upregulation of oxidative stress pathways and nitric oxide-producing enzymes have been shown to play a role in tissue damage and neuronal dysfunction in preclinical sepsis models (Banks et al., 2015; Barichello et al., 2006). The end response of these maladaptive processes likely contributes to the combination of synaptic dysfunction (Hippensteel et al., 2019) and neuronal loss seen in preclinical models of sepsis (Semmler et al., 2007; Zaghloul et al., 2017). Similar to the acute phase of sepsis, these mechanistic factors may also be partly responsible for the long-term effects on cognition in sepsis survivors. For instance, mice that survive exposure to the CLP procedure have demonstrated continued presence of neutrophils in their brain 2 weeks after the procedure along with long-term expression of multiple cytokine and chemokine genes up to 50 days after the procedure (Singer et al., 2016). However, the lasting pathologic changes in the brains of sepsis survivors overall remain poorly characterized and are a necessary area of investigation.

A possible explanation for the long-term change in neuronal function in sepsis survivors could be due to the worsening of an underlying neurodegenerative process such as Alzheimer's disease (AD). One of the hallmarks of AD pathogenesis is the accumulation of the amyloid β (Aβ) peptide in the brain (Holtzman et al., 2011). Aggregation of Aβ into oligomers and senile plaques contributes to the development and progression of cognitive deficits by triggering neuroinflammation, synaptic dysfunction, and neuronal loss (Selkoe and Hardy, 2016). Mounting evidence now suggests that the pathological changes of AD, especially the deposition of Aβ into amyloid plaques, can begin two to three decades prior to symptom onset (Jack Jr. et al., 2010). Biomarker studies using both cerebrospinal fluid (CSF) Aβ42 levels and brain amyloid imaging via positron emission tomography (PET) suggest that a large proportion of cognitively normal elderly individuals have evidence of significant amyloid deposition in their brains (Aizenstein et al., 2008; Peskind et al., 2006). The presence of substantial amyloid plaque deposition on autopsy in similar cohorts of patients with no evidence of cognitive changes further support these findings (Knopman et al., 2003). Given the tendency of critical illness to afflict individuals in the middle to late decades of life, one can extrapolate that many patients treated for sepsis already have ongoing amyloid deposition in the brain. These patients may be at higher risk for worsening of their underlying neurodegeneration when exposed to the inflammatory, neurovascular, and oxidative insults that occur with septic encephalopathy. Understanding how the disease processes of sepsis and AD interact could thus ultimately lead to better understanding of the pathology of cognitive change after sepsis and potentially highlight new directions for therapy.

In this study, we determined how exposure to polymicrobial sepsis influences amyloid plaque deposition in the brain using CLP as a murine model of sepsis. CLP was performed in APP/PS1–21 mice, a model of AD-related β-amyloidosis, and the brains of surviving mice were analyzed two months following the insult. We found that the sepsis-surviving mice had increased levels of hippocampal amyloid load in their brain compared to sham treated animals. Sepsis also increased the extent of astrogliosis and complement activation in the brains of the animals, suggesting ongoing neuroinflammation. Finally, we performed an analysis on the microbial profile in different organs of the mice to determine if changes in bacterial content could potentially be influencing the extent of amyloid deposition. We found that CLP led to significant changes in the gut microbiome, but no changes in brain microbial content were present in the brain. These results highlight that exposure to the inflammatory insult of sepsis could ultimately lead to long-term changes in underlying brain pathology that subsequently contribute to worsening cognitive decline.

2. Methods

2.1. Mice

APP/PS1–21 (APP/PS1) transgenic mice expressing human APP with KM670/671NL Swedish mutations and human PSEN1 with L166P mutation (gift from M. Jucker, University of Tübingen, Tübingen, Germany) on a C57BL6 background were bred with C57BL6 mice (Jackson Laboratory, Bar Harbor, ME) to produce a cohort of heterozygous C57BL6 animals that were used for all experiments. APP/PS1–21 mice were then aged until 2–3 months prior to performing the CLP or sham procedure. An approximately equal number of male and female mice were used for all experiments. All experimental procedures in regards to animal care and experimental design were approved by the Washington University School of Medicine Institutional Animal Care and Use Committee and performed in accordance with the National Institutes of Health guide for the care and use of laboratory animals.

2.2. Sepsis model

Cecal ligation and puncture was performed on all mice as described previously with some modifications (Unsinger et al., 2010). Mice were anesthetized with isoflurane and then underwent a laparatomy via a small incision in the lower left quadrant of the abdomen. For pain control, the mice received an injection of buprenorphine SR (1 mg/kg) injected subcutaneously prior to the procedure. The cecum was then extruded from the abdomen and ligated approximately two-thirds of the distance from the ileocecal junction. The cecum was then punctured once with a 25 gauge needle and stool was extruded from the puncture site to verify patency. The abdomen was then closed via suturing of both the fascial and skin layers, and the mice received a 1 cc injection of 0.9% normal saline injected subcutaneously. All mice then received imipenem (25 mg/kg, subcutaneously) injected 6 h following the procedure. We have found in our laboratory setting that this protocol leads to approximately 50% survival in C57BL6 animals following the procedure. For the sham procedure, the cecum was extruded from the abdomen

but no ligation or puncture was performed. Following the procedure, all animals were housed in normal light/dark conditions at ambient temperature.

2.3. Brain sample collection

Following the CLP or sham procedure, all surviving mice were anesthetized with an intraperitoneal injection of pentobarbital (200 mg/kg) and then perfused with ice-cold PBS containing 0.3% heparin. This was done either 2 months (histological and biochemical analysis cohort) or 5 days (bacterial analysis cohort) after the CLP procedure was performed. For the bacterial analysis cohort, strict attention was paid to aseptic technique during dissection. This included autoclaving all instruments and solutions prior to perfusion and dissection, the use of sterile gloves, and the sterilization of all instruments with 70% ethanol between each animal. Following dissection, one hemibrain was fixed in 4% paraformaldehyde for 48 h at 4 °C and then stored in a 30% sucrose solution in PBS (pH = 7.4) at 4 °C until sectioned. The other hemibrain was dissected into specific brain regions and flash frozen for further biochemical analysis and stored at −80 °C. For the bacteria studies, the cecum and liver of the animals was also extracted and flash frozen for storage at −80 °C.

2.4. Histological staining and image acquisition

Fixed brains were sectioned on a freezing sliding microtome to obtain 50 μm coronal sections. All brain sections were stored in a cryoprotectant solution (30% ethylene glycol, 15% sucrose, 15% phosphate buffer in deionized water). For fibrillar amyloid staining, free-floating sections were washed 3 x in PBS and then incubated in PBS with 0.25% Triton X-100 (PBS-X) for 30 min at room temperature. The sections were then incubated in a solution containing X34 (10 μM X34, Sigma-Aldrich, St. Louis, MO) diluted in a staining buffer (60% PBS, 40% ethanol, 20 mM NaOH) for 20 min at room temperature, and washed 3 times in a wash buffer solution (60% PBS, 40% ethanol) and 2 times in PBS. All sections were then mounted on slides using Fluoromount G and cover-slipped.

For Aβ staining, brain sections were stained with the anti-Aβ_{1-13} antibody HJ3.4 (gift of Dr. David Holtzman, Washington Univ. in St. Louis). Free-floating sections were first washed 3 times in tris-buffered saline (TBS), and then incubated in 0.3% hydrogen peroxide in TBS for 10 min at room temperature. The sections were then washed 3× with TBS and blocked by incubating in 3% milk in TBS with 0.25% Triton X-100 (TBS-X) for 30 min at room temperature. The sections were then incubated in biotinylated HJ3.4 antibody (1:1000 dilution) diluted in 1% milk in TBS-X overnight at 4 °C. The following day, the sections were washed 3× in TBS and developed using a Vectastain ABC Elite kit (1:400, Vector Labs) followed by incubation in a 0.025% 3,3′-deaminobenzidine (DAB, Sigma-Aldrich, St. Louis, MO) containing solution (0.025% DAB, 0.01% NiCl, 0.015% hydrogen peroxide dissolved in TBS). The sections were then washed 3 times with TBS, mounted on slides, and allowed to dehydrate overnight at room temperature. Cresyl Violet counter-staining was then performed by rehydrating the slides in MilliQ water for 2 min and then incubating in Cresyl Violet for 3 min. The slides were then washed sequentially with increasing amounts of ethanol (50%, 70%, 90%, 95%, 100%) followed by Xylene, and coverslips were placed using Cytoseal (ThermoFisher). The slides were then allowed to dry overnight at room temperature prior to imaging.

For glial staining, free-floating sections were washed 3 times in TBS and then blocked by incubating for 60 min in TBS with 0.4% Triton X-100 and 3% donkey serum at room temperature. The sections were then incubated overnight at 4 °C in TBS with 0.4% Triton X-100 and 1% donkey serum solution containing either a GFAP (rabbit, Dako/Agilent, Z0334, 1:3000), S100b (rabbit, Novus, catalog number EP1576Y,1:2000), and IBA1 antibody (goat, Abcam ab5076, 1:500). The following day, the sections were washed 3 times with TBS and incubated for 1 h at RT in TBS with 0.4% Triton X-100 with 1:1000 donkey fluorescent secondary antibodies. The sections were then washed again 3 times with TBS and mounted on slides using Prolong Gold mounting agent (Invitrogen, Carlsbad, CA).

For image acquisition, a Zeiss Axio Imager Z2 fluorescent microscope was used for all wide-field X34 plaque and glia staining. Approximately 12–30 images (1024 × 1024) of the entire hippocampal and upper cortical region were acquired using a 10× objective, and then stitched together using Zeiss Zen software. For some of the glial staining, images were taken on a Zeiss LSM 700 laser scanning confocal microscope with a 63× objective using z-stacks of approximately 25 μm thickness with a step size of 0.5 μm. For Aβ staining, images were obtained using a slide scanner (NanoZoomer, Hamamatsu Photonics) and then exported using the NDP viewer software (Hamamatsu Photonics).

For confocal microscopy, 40× z-stacks were taken using a Zeiss LSM 7000 confocal microscope using 1 μm step sizes. Images were generally obtained from the hippocampal CA1 region.

2.5. Image quantification

X34, HJ3.4, GFAP, S100b, and IBA1 staining were quantified using ImageJ software (NIH). First, the desired regions (hippocampus, cortex, or subregions of the hippocampus) were outlined by drawing ROI's using ImageJ on 8-bit images. Thresholding was then applied to the images to include all of the immunoreactivity for each individual antibody, and this threshold was used for all sections. ImageJ was then used to calculate the percent of area covered. For the analysis, each date point represents one mouse and consists of 2 coronal sections per mouse.

For microglial morphology assessment, Iba1 hyperstacks were opened in ImageJ and different z-planes were used to make a maximum intensity projection (MIP). A ROI was drawn around a single microglia and was used to make a skeleton using ImageJ's skeletonize plugin. The analyze particles function was then applied to gate out small artifacts. The Analyze Skeleton function was then used to count the number of branches. 6–8 microglia were quantified per mouse.

For peri-plaque microglial CD68 colocalization, confocal z-stacks containing X34, Iba1 and CD68 were uploaded to Imaris (version 9, Bitplane Inc.) and surfaces were created for each channel. A colocalized surface channel was then built between Iba1 and CD68. This volume was exported for each picture as well as the volume of X34. The CD69-Iba1 colocalized volume was then divided by the X34 volume from the same image stack for normalization.

2.6. Quantitative PCR

Flash-frozen brain tissue was homogenized in Trizol solution (Life technologies) using a Bullet Blender Homogenizer (Next Advance, Troy, NY). RNA was then extracted and purified using a PureLink™ RNA Mini Kit, Life Technologies, Carlsbad, CA). RNA concentrations were then measured using a Nanodrop spectrophotometer. cDNA was made using a high capacity RNA-cDNA reverse transcription kit (Applied Biosystems/Life Technologies). Microfluidic real-time quantitative PCR measurements were performed by mixing the cDNA with ABI TaqMan primers and ABI PCR Master Mix buffer in a Fluidigm Biomark HD system at the Washington University Genome Technology Access Center. All mRNA measurements. For all mRNA measurements, values were normalized to either β-actin (*Actb*) or *Gapdh* mRNA levels.

2.7. Western blotting

Hippocampal tissue was sonicated in RIPA lysis buffer (ThermoFisher, Waltham, MA) containing complete protease inhibitor (Roche Life Sciences, Indianapolis, IN), and then spun down at 15,000 x*g* for 15 min at 4 °C. The supernatant was then collected and the protein concentrations in the samples were measured using a Pierce BCA Protein Assay Kit (ThermoFisher), and samples containing equal amounts of

protein were loaded into nuPAGE 4–12% Novex Gels (ThermoFisher) and run using SDS running buffer. The proteins were then transferred to a PVDF membrane using an XCell II™ transfer device (ThermoFisher). The membranes were then blocked by incubating in 5% milk in TBS-T (Tris-buffered saline with 0.125% Tween 20) for 1 h at room temperature. Blots were then probed for either APP (6E10 antibody, 1:1000, Biolegend) or Tubulin (1:50,000, Sigma Aldrich). Protein signal from the membranes was obtained using a Lumigen TMA-6 ECL detection kit (Lumigen, USA) and quantified using Image J software (NIH).

2.8. 16S rRNA sequencing and analysis

Whole gDNA was isolated from cecal, liver, plasma, and brain (cortex and hippocampus) samples using TRIzol reagent (Invitrogen 15,596,026). Thawed samples were first transferred to bead beating tubes from the Powersoil Pro kit (Qiagen 47,014), followed by addition of 1 mL TRIzol reagent to each sample and homogenization in a Mini-Beadbeater-24 (Biospec Products) with the following parameters: 2000 rpm for 2 min, followed by 1 min on ice and another 2 min cycle at 2000 rpm. Homogenized samples were spun down in a mini spin centrifuge and supernatants were used as input for gDNA purification following the TRIzol manufacturer's protocol. In the final step DNA was solubilized with 8 mM NaOH and pH adjusted to 7–8 with 1 M HEPES and 1 mM EDTA. DNA was quantified using a Qubit fluorometer dsDNA HS Assay (Invitrogen Q32851) and stored at −20 °C.

The purified gDNA was used as template for 16S rRNA sequencing. We performed sequencing of the variable region (V4) of the 16S rRNA gene using 515F/806R PCR primers including Illumina flowcell adapter sequences to amplify the V4 region using the Earth Microbiome Protocol (Caporaso et al., 2012) (described in more detail here: http://www.earthmicrobiome.org/ emp-standard-protocols/16 s/). Briefly, the following 25 μL reaction was prepared in 96-well plates: 10 μL H20, 12.5 μL Taq Hot-Start DNA Polymerase (Takara R028A), 1 μL forward primer (10 uM), 1 μL reverse primer (10 uM), 0.5 μL template DNA (1 ng/uL). PCR cycle temperatures were as follows: 98C for 30 s, then 35 cycles of [98C for 10 s, 50C for 30 s, 72C for 30 s], then 72C for 2 min. PCR reactions were carried out in triplicate for each reaction. In addition, a template-less control reaction was carried out for each primer pair. PCR products were assessed via gel electrophoresis to verify the amplicon size and absence of contamination, then were quantified using the PicoGreen kit (Invitrogen P11496), following the manufacturer's protocols. 16S rRNA gene amplicons were sequenced by 2 × 250 bp paired-end sequencing on the Illumina MiSeq platform using custom primers (read 1: 5′-TAT GGT AAT TGT GTG CCA GCM GCC GCG GTA A-3′; read 2: 5′-AGT CAG TCA GCC GGA CTA CHV GGG TWT CTA AT-3′; and index: 5′-ATT AGA WAC CCB DGT AGT CCG GCT GAC TGA CT-3′) at a loading concentration of 8pM with 25% PhiX spike-in.

For each mouse, reads from the hippocampus and cortex samples were concatenated. Brain, liver, plasma, and cecal reads were analyzed using the DADA2 package (v1.12) in R (Callahan et al., 2016) which has built-in quality-filtering, dereplication, and removal of chimeric sequences, to identify amplicon sequence variants (ASVs). The R package DECIPHER (v12.4.0) (Wright, 2015) was used in conjunction with the SILVA SSU rRNA database (release 132) (Quast et al., 2013) for taxonomic assignation. Contaminant eukaryotic reads from spuriously amplified mouse mitochondrial DNA were removed. Despite relatively even raw read counts, after these steps bacterial read counts per sample ranged from ~200 (e.g. in the liver of a mouse that received sham surgery) to ~70,000 (e.g. in the cecum of a mouse that received CLP). Rarefaction analysis was performed using the vegan package (v2.2–5) in R {https://cran.r-project.org/web/packages/vegan/vegan.pdf} and only samples with a terminal rarefaction slope less than 0.01 were retained for downstream analysis, removing 3 of 84 samples. The R package phylosEq. (v1.28.0) (McMurdie and Holmes, 2013) was used to collate the DADA2 output (ASV counts and taxonomic identity) with sample metadata in order to calculate and compare alpha diversity metrics (richness and Shannon's H), relative abundances of taxa per sample, and to carry out principal coordinates analysis on the Bray-Curtis dissimilarities between samples. PERMANOVA tests for compositional differences (by Bray-Curtis dissimilarity) between treatment groups were carried out for each tissue type using the adonis function in the vegan package (v2.2–5). To identify taxa with significantly different relative abundances between treatment groups in the ceca, we used the linear discriminant analysis effect size method LEfSe (Segata et al., 2011) via the Galaxy web application (https://huttenhower.sph.harvard.edu/galaxy/), using treatment as the class, no subclass, and 0.01 *p*-value thresholds for the Kruskal-Wallis and Wilcoxon test steps.

2.9. Statistical analysis

Unless stated otherwise, statistical analyses were performed using GraphPad Prism v8.02. For most studies, an unpaired two-tail *t*-test was performed to test for statistical significance between two groups, with significance assigned for $P < 0.05$. All data is presented as the mean ± standard error of the mean unless otherwise stated. For survival analysis, a log-rank Mantel-Cox test was used to compare between the different cohorts.

3. Results

3.1. CLP increases fibrillar amyloid burden in the hippocampus

To address whether polymicrobial systemic sepsis influences the extent of amyloid deposition in the brain, we performed CLP using the APP/PS1–21 transgenic mouse model of AD-related Aβ deposition. APP/PS1 mice have mutations in amyloid precursor protein (APP) and presenilin 1 (PS1) causing increased production of Aβ and accelerated deposition of amyloid plaques beginning around 6 weeks of age in the cortex and 2 months of age in the hippocampus (Radde et al., 2006). CLP was performed on mice at 2 months, an age at which amyloid deposition is just beginning in the hippocampus in this model. Following the procedure, all surviving mice were aged for another two months at which point the brains were extracted and analyzed.

We performed a moderate form of CLP that led to an approximate mortality rate of 50% in our laboratory environment (Supp. Fig. 1). To evaluate whether the level of mortality and correlatively the level of systemic insult was influenced by the APP and PS1 transgenes, we compared the survival rate using the same CLP procedure on both APP/PS1 and Wt mice. The survival rate between both APP/PS1 and WT mice was not different (50% vs 55%, $p = 0.69$).

To evaluate the extent of amyloid deposition in the brains of surviving mice, the tissue of both CLP and sham treated mice were stained with the X-34 compound. X-34 is a highly fluorescent derivative of Congo Red that detects the β-pleated sheet conformation present primarily in the compact core of mature fibrillar amyloid plaques (Ikonomovic et al., 2006). Mice that survived the CLP procedure had a significant higher level of X-34 signal in the hippocampus compared to sham mice (Fig. 1A and C, 0.35 vs 0.22%, $p < 0.05$). The amount of X-34 staining in the cortex was not different between CLP and sham treated animals (Fig. 1B and C, 1.41 vs. 1.55%, $p = 0.43$), suggesting a region-specific effect of sepsis on amyloid deposition. We then analyzed subregions of the hippocampus to determine if the effect of CLP on hippocampal amyloid deposition was uniform. We found that CLP increased the amount of X-34 signal in the dentate gyrus compared to a sham procedure (0.79% vs. 0.47%, $p = 0.0082$), but not in the CA1 area (0.2% vs. 0.23%, $p = 0.72$) (Fig. 1D). These results therefore highlight that the overall increase in hippocampal amyloid deposition with CLP is heavily driven by changes in specific subregions. Finally, we evaluated the effect of CLP on total Aβ brain levels in surviving mice using an N-terminal Aβ antibody (HJ3.4). Interestingly, CLP did not significantly alter the amount of Aβ-reactivity in either the hippocampus or cortex compared to sham-treated mice (Supp. Fig. 2A and B, hippocampus, 0.33% vs

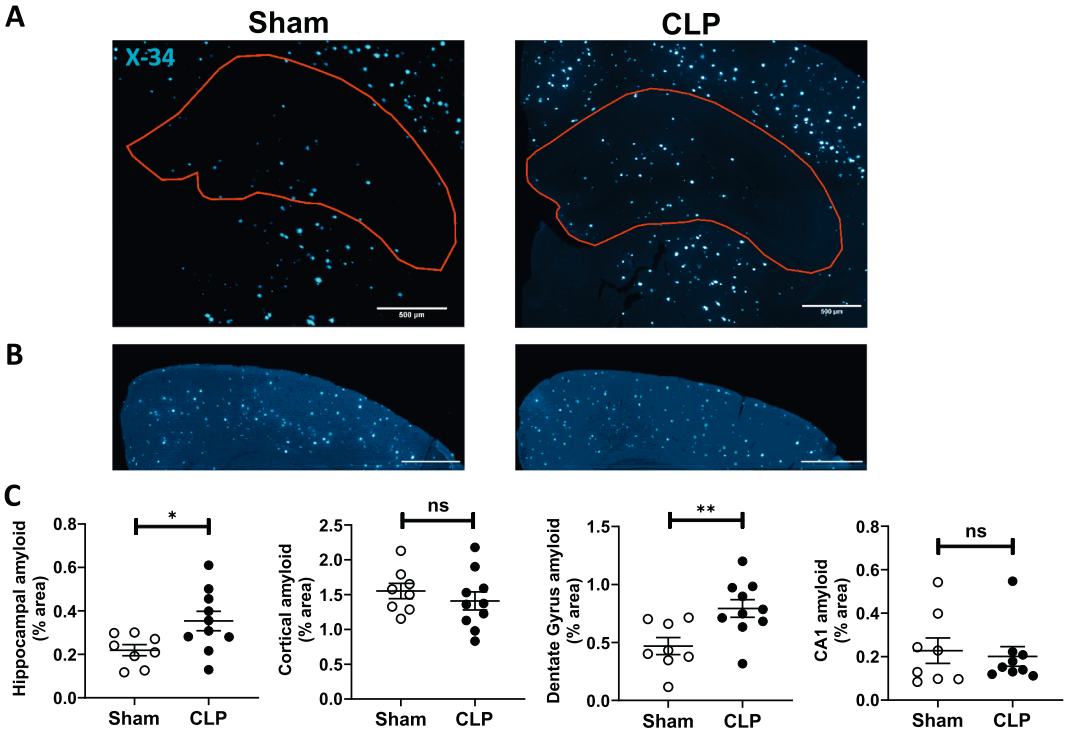

Fig. 1. Increased fibrillar amyloid in sepsis-surviving APP/PS1 mice. Representative X-34 stained (A) hippocampal and (B) cortical images from the sectioned brain tissue of APP/PS1 mice subjected to either a sham procedure or CLP (scale bar = 500 μm). (C) The percentage of hippocampus stained with X-34 was significantly increased in CLP treated mice (0.35 vs. 0.22, $p < 0.05$, $n = 8$ animals for sham group, $n = 10$ animals for CLP group), while the percentage of cortex stained with X-34 was not different (1.41 vs 1.55, $p = 0.43$). (D) In comparing different regions of the hippocampus, the percentage of the dentate gyrus area of the hippocampus stained with X-34 was significantly increased (0.79% vs. 0.47%, $p = 0.0082$) while the percentage of the CA1 region stained with X-34 was not altered in comparing CLP to sham-treated mice (0.20% vs 0.23%, $p = 0.72$).

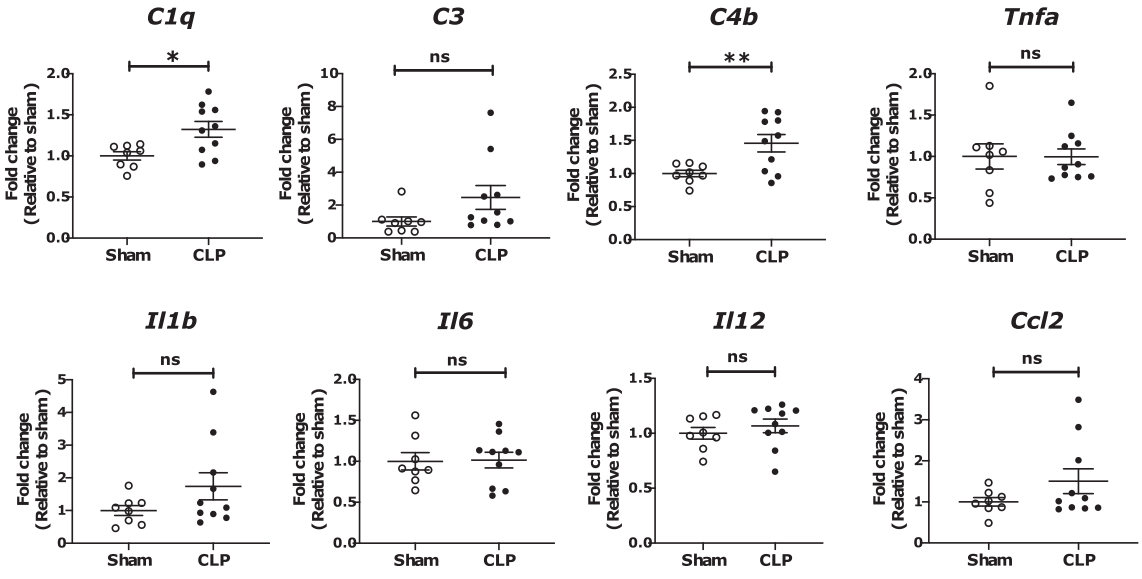

Fig. 2. CLP induces complement gene expression but not other inflammatory mediators in APP/PS1 mice. qPCR quantification of transcript levels for several complement genes and inflammatory mediators in hippocampal tissue from sham or CLP mice, 2 months after surgery. $N = 8$ sham, 10 CLP mice. p values: * <0.05, ** <0.01 by 2-tailed t-test, ns = not significant.

0.28%, $p = 0.43$, cortex, 3.02% vs 3.28%, $p = 0.78$). The discrepancy in the hippocampal changes in X-34 and total Aβ staining following CLP suggests that sepsis may have a propensity to trigger the conversion of Aβ into a more compact fibrillar structure that is primarily detected by the X-34 compound.

3.2. CLP causes mild immune activation in APP/PS1 mice after 2 months and does not change amyloid precursor protein (APP) processing

Long-term immune activation following CLP could play a role in enhancing the formation of amyloid in the brain. A prior study has shown that the expression levels of multiple cytokines and chemokines

remain elevated for up to 50 days after survival from CLP (Singer et al., 2016). Using quantitative PCR, we evaluated whether the expression of any immunological activators remain elevated in APP/PS1 mice following CLP. Sepsis-surviving mice overall demonstrated evidence of mild chronic immune activation in the brain, with significant elevations observed in complement factors *C1q* and *C4b* (Fig. 2). Importantly, *C4b,* which encodes complement protein C4, has been previously demonstrated to be increased in human AD brain, and to promote Aβ aggregation in vitro (Zhou et al., 2020). A trend toward increased levels of *C3*, *Il1b* (encoding interleukin 1-β), and *Ccl2* was also observed, while several other inflammatory transcripts were unchanged.

Inflammation and certain pro-inflammatory cytokines are capable of increasing the activity of the enzymes α-secretase and beta-secretase 1 (BACE1), both of which play a critical role in the processing of the amyloid precursor protein (APP) into the Aβ peptide (Avramovich et al., 2002; Sastre et al., 2003; Yamamoto et al., 2007). Measuring changes in full-length APP along with its cleavage products is an indirect method to determine alterations in Aβ synthesis. Therefore, to assess whether increased Aβ production could be functioning in driving the increased amyloid levels observed in CLP-surviving mice, we evaluated the amount of hippocampal full-length APP and the C-terminal fragment of APP resulting from BACE1 cleavage of APP following CLP. We did not observe any differences in either APP or its C-terminal fragments (C83 and C99) in comparing CLP to sham-treated APP/PS1 mice (Fig. 3A, for full gel images see Supp. Fig. 3). We then measured the transcript level of the APP processing genes *Psen1*, *Psen2*, and *Bace1* in CLP and sham-treated APP/PS1 mice and observed no changes (Fig. 3B). Taken together, these results emphasize that sepsis does not result in any long-term effects on APP processing associated with changes in Aβ production.

3.3. Hippocampal astrogliosis, but not microgliosis, increases in APP/PS1 mice following CLP

Reactive astrogliosis and microgliosis are hallmarks of AD pathology and likely play an important role in regulating the amount of amyloid deposition in the brain (Heneka et al., 2015). Furthermore, extensive gliosis has been described in multiple preclinical models of sepsis and is postulated to be a driving factor in the acute and likely chronic neuroinflammatory process (Henry et al., 2009; Michels et al., 2015). To assess if CLP influences the amount of chronic glial reactivity in the brains of APP/PS1 mice, we first analyzed the levels of GFAP in the brains of the surviving animals. Immunohistochemistry for GFAP (Fig. 4A) demonstrated a significant increase in hippocampal astrocyte reactivity with CLP (Fig. 4B, 4.3% vs. 2.26% for CLP and sham, $p = 0.01$). To determine whether the changes in glial activity were strictly driven by alterations in amyloid load versus a diffuse overall increase in cellular reactivity, we also normalized the amount of GFAP reactivity to the amount of X-34 plaque load (Fig. 4B). After normalization, there was still a strong trend toward increased astrogliosis in CLP compared to sham-treated mice which was significant by 1-tailed but not a 2-tailed *t*-test (13.75 vs 9.26, $p = 0.039$ for 1-tailed and 0.078 for two-tailed). This suggests that the increase in observed hippocampal astrocyte activation following CLP is predominantly centered around increased fibrillar plaque levels, but that CLP may also mildly exacerbate diffuse astrocyte activation across the hippocampus independent of plaque amount. We then co-stained a random subset of hippocampal brain tissue with GFAP and the astrocytic marker S100β to measure whether the increased GFAP levels are due to an increase in total astrocyte numbers (Fig. 4C). Interestingly, we found that while GFAP reactivity increased in the CLP brains, there was no significant difference in S100β levels between CLP and sham mice (7.44% vs 9.49%, $p = 0.11$) (Fig. 2D). Taken together, these results highlight that total astrocyte cell numbers likely do not change with CLP, but the total amount of activated astrocytes (as evidenced by GFAP levels) is increased. To further analyze whether a specific subtype of reactive astrocyte was the predominant cell-type in the brains of CLP-surviving mice, we analyzed several gene transcripts relevant in A1 and A2 astrocyte polarization (Liddelow et al., 2017). Consistent with our staining results, we found the mRNA level of *Gfap* to be significantly increased in CLP mice along with the pan-reactive astrocyte gene *Vim* (encoding for the protein vimentin) (Supp. Fig. 4). However, no difference were observed in the genes encoding *Serpina3n*

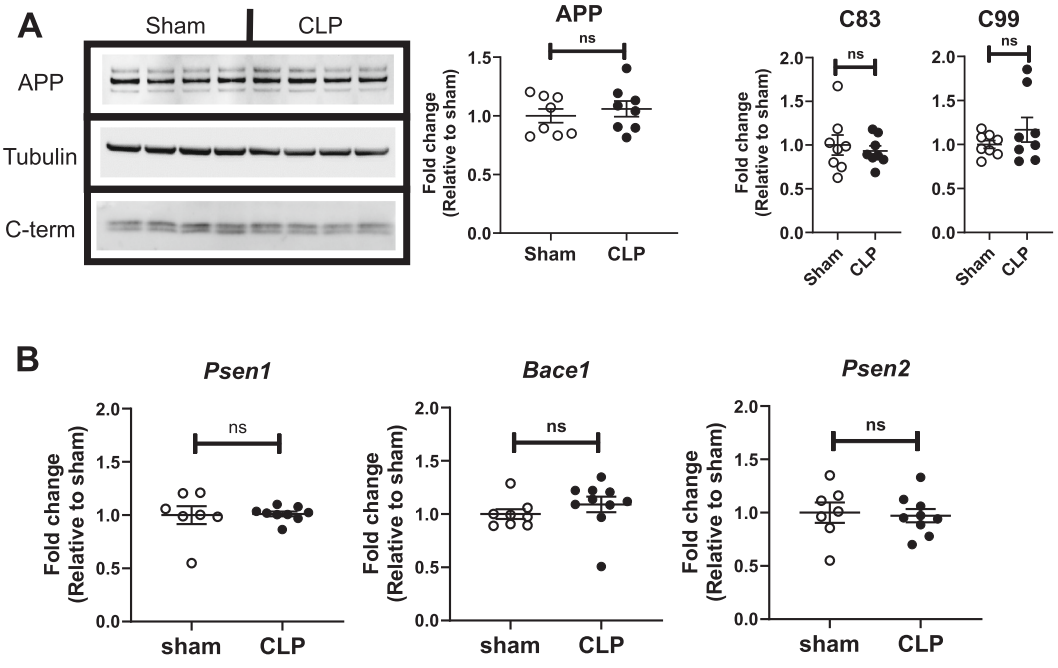

Fig. 3. CLP does not alter APP processing in surviving APP/PS1 mice. (A) Immunoblot analysis of amyloid precursor protein (APP) and the C-termini fragments of APP (C99 and C83) from hippocampal lysates of APP/PS1 mice subjected to either sham or CLP procedure. One representative gel is shown. Tubulin served as a loading control. (B) qPCR assessment of APP-processing transcripts demonstrates no change in hippocampal mRNA levels between sham and CLP brain tissue. p values: * <0.05, ** <0.01 by 2-tailed t-test.

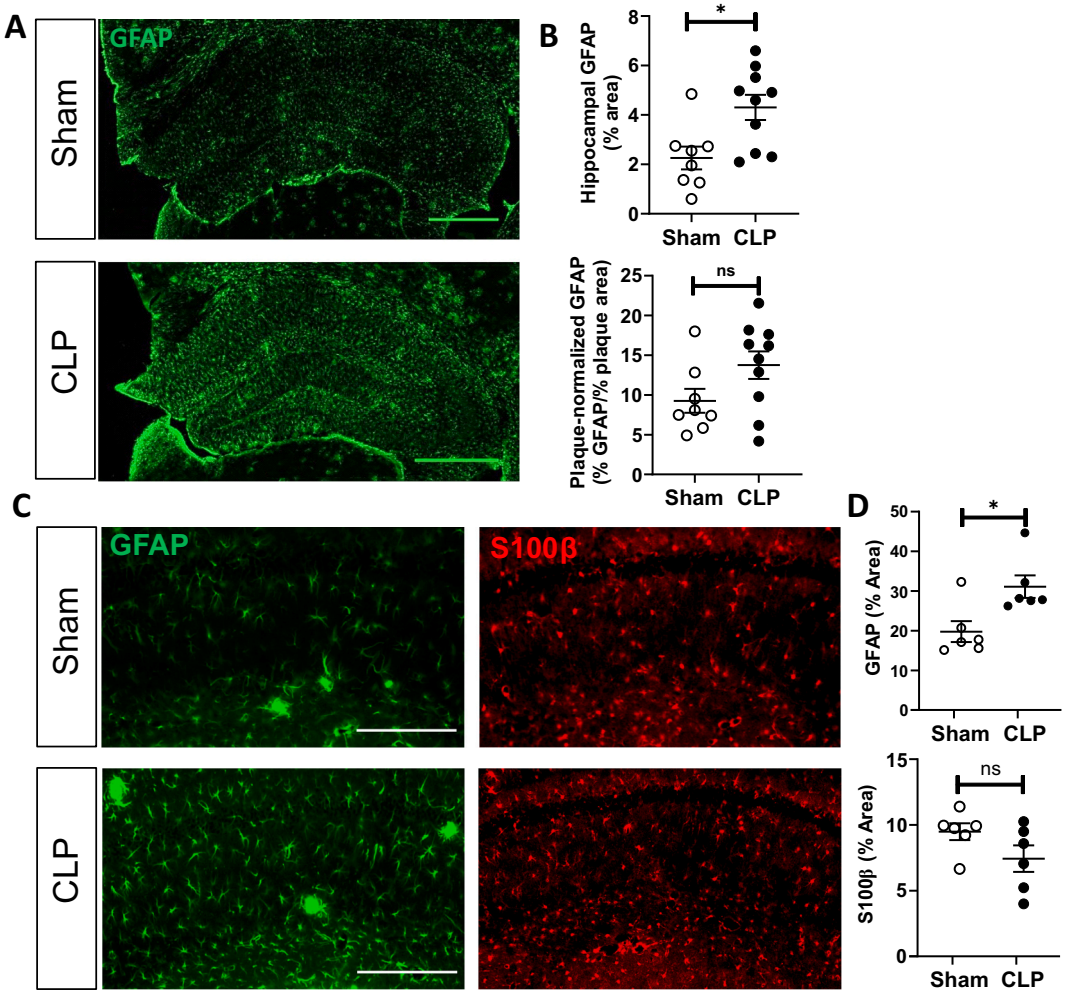

Fig. 4. CLP increases chronic astrocyte activation but not total astrocyte numbers in the hippocampus of APP/PS1 mice. (A) Representative brain images of GFAP and Iba1 from APP/PS1 mice 2 months after either a sham procedure or CLP (scale bar = 500 μm). (B) Quantification of GFAP immunostaining demonstrates an increase in GFAP (4.3 vs 2.26, $p = 0.01$) following CLP. Also shown is the normalization of GFAP levels to the amount of plaque in the brain. Staining was then repeated on a subset of the sham and CLP-treated APP/PS1 mice with the astrocytic markers GFAP and S100β. (C) Representative images of hippocampal sections are shown (scale bar = 100 μm). (D) Quantification of GFAP was again increased following CLP (19.88% for sham versus 31.1% for CLP, $p = 0.015$), while S100β immunostaining did not demonstrate an increase in immunoreactivity (9.49% for sham versus 7.44% for CLP, $p = 0.11$).

or the A1/A2 astrocytic genes *Psmb8*, *Gbp2* (A1-specific), and *Dd14* (A2-specific). Therefore, the astrocytic activation present after CLP in the APP/PS1 mice does not appear to show evidence of a definitive A1 or A2 polarization.

Chronic microglial activation has been described in several different models of murine sepsis (Henry et al., 2009; Singer et al., 2016). To determine if total microglial cell numbers are increased in the hippocampus of APP/PS1 that survive sepsis, we used immunostaining to measure the amount of Iba1 immunoreactivity in the brain of sham and CLP-treated mice (Fig. 5A). Interestingly, we observed no statistical differences in total Iba1 staining (6.36% of total hippocampal area for CLP mice compared to 5.06% for sham mice, $p = 0.3$) or plaque-normalized Iba1 levels (19.6 vs 20.8 for sham and CLP-treated groups, $p = 0.78$) (Fig. 5B). Given Iba1 levels may not specifically detect activated microglia, we also analyzed the extent of phagocytic activation in microglia and assessed for changes in microglial morphology. CD68 is a lysosomal protein expressed in macrophages and is known to be present in high levels in activated microglia. To assess for microglial-specific changes in phagocytic activation, we co-stained brain sections from a subset of sham and CLP-treated APP/PS1 mice with CD68, Iba1, and X34 (Fig. 5C). Notably, a predominant amount of the CD68 immunoreactivity was localized around plaque structures. No significant difference was observed in CD68 levels localized to Iba1 cells surrounding plaques when comparing sham to CLP-treated mice. The morphology of activated microglia also differs from resting microglia, as activated cells tend to become more ameboid in shape with fewer and thicker cellular processes (Davis et al., 1994). To assess for changes in microglial morphology, we performed a skeletonized quantification of the degree of microglial branching in both sham and CLP mice. While there was a trend toward a decreased number of branches per microglia in CLP-treated mice, the difference was not significant (Supp. Fig. 5). Finally, a unique subset of cells known as disease-associated microglia (DAM) have been described in neurodegenerative conditions and may play a role in regulating the progression of plaque deposition (Keren-Shaul et al., 2017). Interestingly, we found that a set of DAM-associated transcripts (including *Cybb* and *Clec7a*, with *Trem2* showing a trend toward increase) were increased in the hippocampus of APP/PS1 mice that survived sepsis (Fig. 5D), suggesting there may be subtle changes in microglia activation present in the brain after sepsis.

Finally, in order to determine whether CLP itself leads to long-term gliosis that could impact plaque formation, we analyzed the amount of astrocyte and microglial activation in WT mice subjected to the CLP procedure. Two months following either CLP or sham, the brains from surviving mice were extracted and stained for either GFAP or Iba1. No

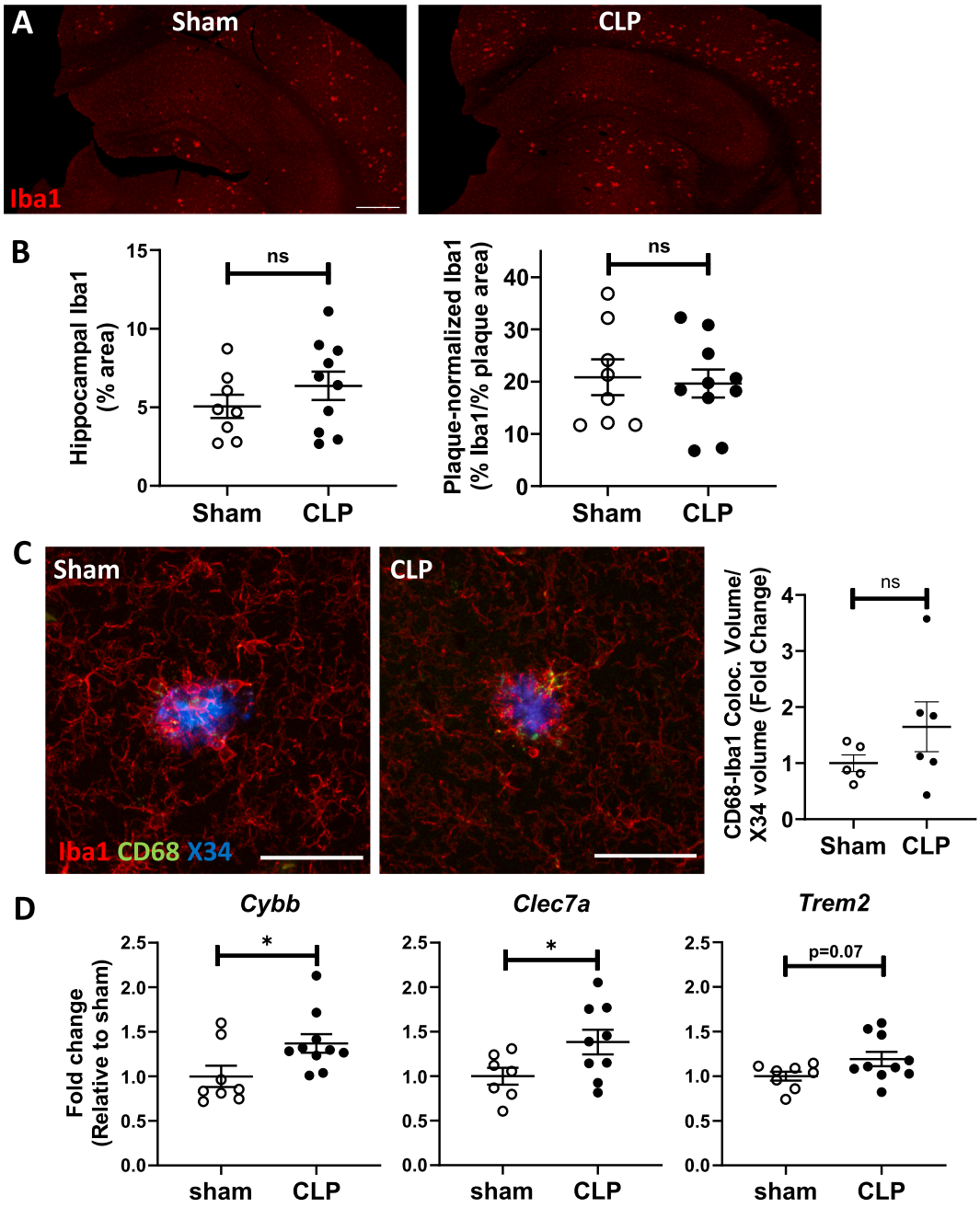

Fig. 5. CLP does not change hippocampal microglial activation but does increase disease associated microglial (DAM) gene transcript expression. (A) Representative brain images of Iba1 immunostaining from APP/PS1 mice 2 months after either a sham procedure or CLP (scale bar = 500 μm). (B) Quantification of hippocampal Iba1 immunostaining does not show evidence of changes in microglial levels (5.06 vs 6.36, $p = 0.296$) following CLP. Also shown is the normalization of GFAP levels to the amount of plaque in the brain. To assess for changes in the phagocytic function of microglia after CLP, the amount of CD68 localized to plaque-associated Iba1-positive cells was quantified (C) Representative images of hippocampal sections are shown (scale bar = 50 μm). No significant difference was observed in microglial-associated CD68 between CLP and sham-treated mice ($n = 6$ animals per group, images taken from the CA1 region) (D) qPCR quantification of transcript levels for several DAM genes from sham or CLP mice. p value: * <0.05.

significant difference was observed in either GFAP (Supp. Fig. 6A, 3.97 vs 4.00% for sham and CLP, $p = 0.93$) or Iba1 (Supp. Fig. 6B, 2.93 vs. 3.74 for sham and CLP, $p = 0.15$) when comparing CLP to sham treated mice without plaques. In summary, these data demonstrate that CLP leads to a significant increase in hippocampal astrogliosis in APP/PS1 that appears to be in part dependent upon the elevation in amyloid deposition.

3.4. Effect of CLP on the microbiota of APP/PS1 mice in different organs

Recently, changes in the gut microbiome have been implicated in modulating amyloid plaque deposition in mice and altering the neuroinflammatory response to plaques (Dodiya et al., 2019; Minter et al., 2016; Minter et al., 2017). The microbiota present in the brains of patient's who die of sepsis also has been shown to differ from patient's who die of other causes (Singer et al., 2018). We therefore decided to evaluate for any differences in bacterial microbiome composition between CLP and sham treated APP/PS1 mice to determine if these changes could

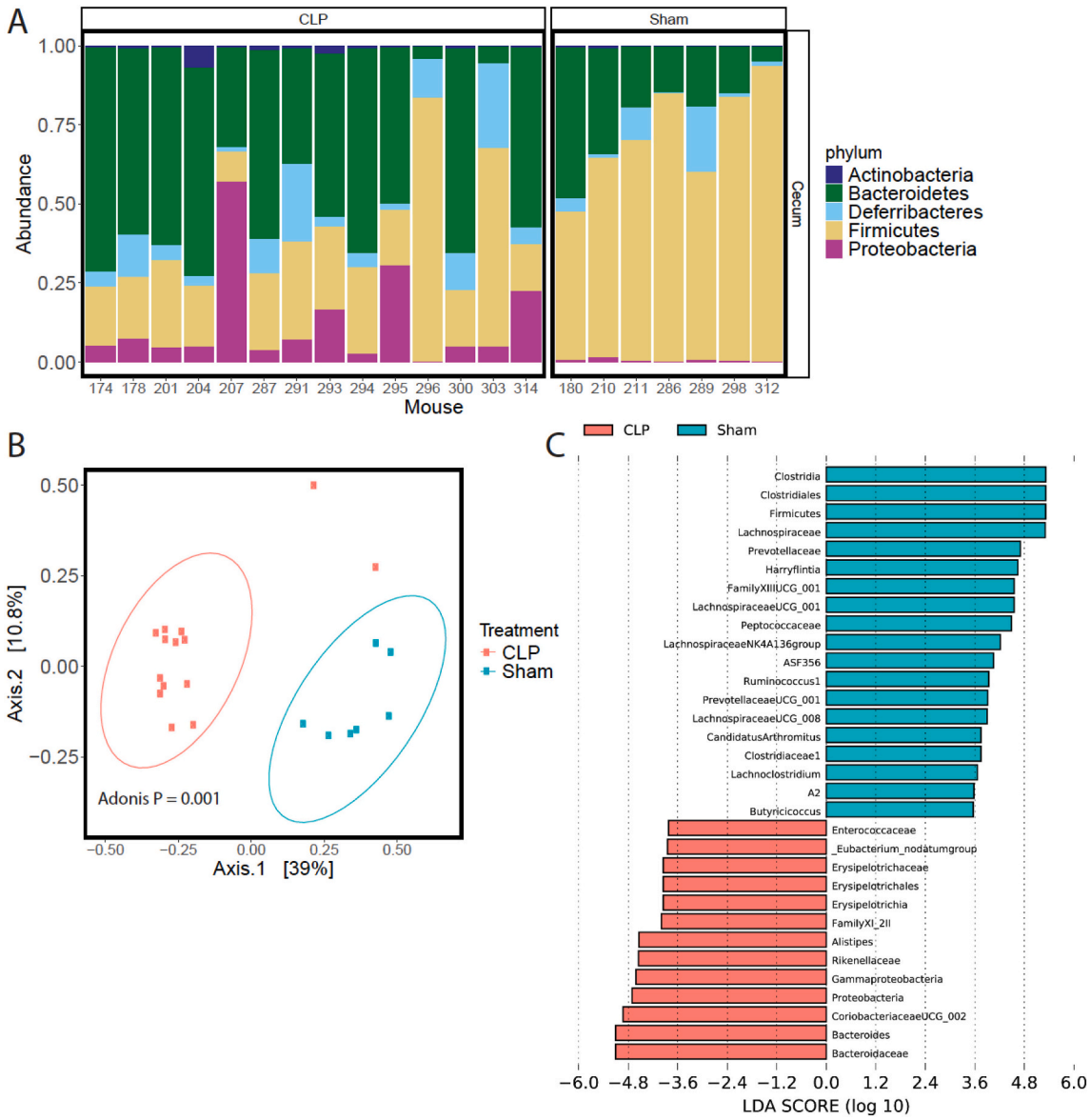

Fig. 6. Comparison of cecal microbiomes from APP/PS1 mice that received CLP or sham surgeries. (A) Relative abundance stacked barplots of cecal taxa from CLP or sham-treated mice at the phylum level. (B) Principal coordinates analysis ordination of cecal microbiomes based on Bray-Curtis dissimilarities with 95% confidence ellipses by treatment. Adonis: PERMANOVA *p*-value from the adonis function in the vegan R package. (C) Discriminatory taxa significantly associated with CLP or sham surgery in the cecum identified by the linear discriminatory analysis effect size method (LEfSe). (N = 14 CLP and 7 sham surgery mice).

be influencing plaque levels and inflammation in the brain. We carried out 16S rRNA sequencing of cecal, brain, liver, and plasma samples harvested from mice five days after CLP or sham surgery. Microbial compositions were significantly different in the ceca of mice that received CLP compared to sham surgery (PERMANOVA $p = 0.001$), with CLP cecal samples exhibiting increased relative levels of Bacteroidetes and Proteobacteria with a concomitant decrease in Firmicutes (Fig. 6), and a significant decrease in overall species richness ($p = 0.04$, Wilcoxon). However, bacterial microbiome compositions were not detectably different in the brain, liver, or plasma samples between treatment groups (Supp. Fig. 7). Thus, we found that our CLP model causes pronounced alteration in the gut microbiome but no detectable changes in brain microbiota composition at this timepoint.

4. Discussion

Survivors of sepsis often have long-term changes in their cognition and memory that cause significant disability well after recovery from their initial illness (Iwashyna et al., 2010). The pathophysiology underlying the acute effects of sepsis on the brain has been extensively addressed in both animal models and clinical studies (Sonneville et al., 2013; Widmann and Heneka, 2014). However, the long-term molecular and pathologic sequela in the brain following sepsis remain poorly characterized. In this study, we analyzed whether the neurologic insults of sepsis influence the progression of the pathologic changes associated with Alzheimer's disease. We have discovered that systemic sepsis alters the severity of the pathology present in a mouse model of β-amyloidosis in mice that survive their illness. Specifically, we found that mice that survive CLP have a significantly higher fibrillar amyloid plaque load in their hippocampus compared to sham animals. CLP also led to long-term neuroinflammation in brains of surviving mice, with significant increases in astrocyte activation and complement *C4b* gene expression. Finally, significant perturbations in the gut microbiota of APP/PS1 mice were observed after CLP, suggesting sepsis may shift the microbiome to a pro-amyloidogenic and neuroinflammatory state. Taken together, these results suggest that the chronic cognitive changes following

polymicrobial sepsis may be secondary to the progression of an underlying neurodegenerative disease.

Imaging and biomarker studies continue to highlight that AD pathology develops years prior to the onset of clinical symptoms. The first detectable manifestation of the disease is the deposition of Aβ into amyloid plaques, as evidenced by decreased CSF Aβ42 levels and increased fibrillar amyloid deposits in the brain measured with PiB-PET imaging (Jack Jr. et al., 2010). Studies suggest that this process can start 15 to 20 years prior to individuals meeting the clinical threshold of an AD diagnosis (Bateman et al., 2012; Villemagne et al., 2013). Preclinical AD is very common among people over 65 and increases in prevalence with age (Jack Jr. et al., 2019). In fact, a recent study modelling preclinical AD suggests that over 46 million Americans may have some evidence of AD changes in their brain (Brookmeyer et al., 2018). Given sepsis predominantly affects the elderly (Martin et al., 2006), a great number of patients treated for an episode of sepsis likely possess the early pathological changes of preclinical AD in their brain. It is therefore not unreasonable to postulate that the neurological insults of sepsis, including neuroinflammation and alterations in blood flow, could produce long-standing effects on the progression of the underlying neurodegeneration. In this study, we modeled this clinical scenario in an animal model by subjecting APP/PS1 mice to CLP at 2 months of age. At this timepoint, this APP/PS1 model are just beginning to demonstrate the initial signs of amyloid deposition in the brain but have no evidence of memory deficits on behavioral tasks (Radde et al., 2006). Our finding that hippocampal fibrillar plaque load is increased 2 months following the septic insult has important translational implications in that it suggests sepsis could promote plaque deposition and neuroinflammation in older people with preclinical AD, potentially accelerating the onset of symptomatic cognitive decline. Future studies with human sepsis-survivors employing modern AD biomarkers, such as CSF Aβ measures or amyloid PiB-PET imaging, will ultimately be needed to address this issue.

Prior studies have addressed the extent to which a systemic inflammatory challenge influences AD pathology primarily by injecting mouse models of Aβ-amyloidosis with intraperitoneal LPS. These experiments have yielded conflicting results that seem to depend upon both the dose, timing, and frequency of LPS administration (Tejera et al., 2019; Wendeln et al., 2018). LPS administration has historically been used as a model of sepsis as well, though with significant limitations. These include the short temporal profile and large intensity of the inflammatory response along with the emphasis on one distinct inflammatory pathway (TLR4). For this study, we chose CLP as our murine model of sepsis. CLP has been postulated to be a more clinically relevant model of sepsis from a pathophysiologic standpoint given it causes a robust polymicrobial infection with a more sustained inflammatory insult. To our knowledge, the only study to assess the effect of CLP on AD pathogenesis demonstrated that wild-type rats have increased soluble Aβ levels in the brain 30 days following the septic insult (Gasparotto et al., 2018). Our study is the first to show that CLP affects the accumulation of amyloid plaques in the brain using a murine model of human β-amyloidosis.

Our data suggest that sepsis interacts with amyloid pathology to promote inflammation in the mouse brain. In APP/PS1–21 mice, there were several inflammatory transcripts which were persistently elevated 2 months after CLP, suggesting that CLP exacerbates plaque-related inflammation. Transcripts which were increased by CLP include the complement genes *C1q* and *C4b*. C1q has been widely demonstrated to be increased in human AD and APP/PS1 mouse models, and has been implicated in modulating plaque formation and Aβ-mediated synapse loss. *C4b* transcript increases with aging in mouse astrocytes, and was recently identified in a single-nucleus RNA sequencing study of transcripts increased in human AD brain (Zhou et al., 2020). That study suggested that *C4b* was expressed by oligodendrocytes, and demonstrated that C4 protein (the protein product of the mouse *C4b* gene) can seed Aβ aggregation in vivo, suggesting that inflammatory C4 production may promote plaque formation. While the exact mechanisms are not yet clear, persisting inflammation in the brains of APP/PS1–21 after sepsis may contribute to increased fibrillar plaque formation.

While not definitive, our data also suggest that gastrointestinal causes of sepsis, such as bowel perforation, which are most common in the elderly, could lead to gut microbiome perturbations which could potentially promote amyloid plaque formation and AD. Altering the mouse gut microbiome with antibiotics in an APP/PS1 mouse models (including APP/PS1–21 mice) can decrease amyloid plaques and plaque-related microglial activation (Dodiya et al., 2019; Minter et al., 2016; Minter et al., 2017). This effect is more apparent in male mice, and can be reversed by fecal transplant from wild-type mice (Dodiya et al., 2019). In a different study, a drug (sodium oligomannate) that reduces gut dysbiosis was demonstrated to improve cognition and reduce neuroinflammation in the 5XFAD mouse model of AD-associated amyloidosis, though the relevance of the specific bacterial phyla altered with this drug remains a topic of some controversy (Wang et al., 2019). The mechanism underlying the neuropathological changes in these studies is unknown, but one possibility is a change in the overall systemic inflammatory state that lessens the likelihood of amyloid formation in the brain. Gut microbiome changes have been described not only in APP/PS1 mice, but also in humans with mild cognitive impairment and with AD (Wang et al., 2019). Thus, sepsis-related microbiome changes could influence amyloid deposition and neuroinflammation, though specific bacterial changes which may drive disease need further elucidation.

In the present study, we found that the composition of the gut microbiota was chronically altered in the setting of CLP, with an increased prevalence of bacterial species from the Bacteroidetes and Proteobacteria phyla and a decreased prevalence of Firmicutes. The relevance of these specific microbiota changes on the brain remain unclear, but several findings suggest bacteria from these phyla may regulate neuropathology in the brain. A recent study demonstrated that infection of mice with *Porphyromonas gingivalis*, a member of the Bacteroidetes phylum, leads to increased levels of Aβ in the brain (Dominy et al., 2019). Relevant to our findings, Dodiya and colleagues recently showed that a multi-antibiotic regimen lowered amyloid plaque burden in APP/PS1–21 mice (the same model used in our studies), while at the same time reducing the relative levels of Bacteroidetes and increasing Firmicutes species (Dodiya et al., 2020). While not conclusive, these data suggest that further inquiry into the relative proportions of different bacterial phyla and their effects on amyloid plaque deposition is needed. It has also been postulated that increased relative levels of Proteobacteria lead to a state of heightened dysbiosis and increased levels of systemic inflammation (Shin et al., 2015). This pro-inflammatory state could then stimulate changes in the brain either through direct transmission of inflammatory mediators across the blood-brain barrier or communication from the gut to the brain through inflammatory reflex pathways mediated through afferent pathways such as the vagus nerve. Future experiments will need to address precisely how the gut-brain axis is altered after sepsis, and what role changes in the microbial content play in this process.

Finally, it has been proposed that a previously unknown function of Aβ may be to act as an anti-microbial peptide in the brain. Injection of certain bacterial species into the brain leads to the accumulation of Aβ around the bacteria, and ultimately seeds amyloid plaques in APP transgenic mice (Kumar et al., 2016; Soscia et al., 2010). In terms of a direct link between brain bacteria and sepsis, transient seeding of the brain with gut bacteria has been reported in mice following CLP (Singer et al., 2018). Thus, we initially hypothesized that gut bacteria entering the brain after CLP may act to seed amyloid plaques in our model. However, we did not find a clear signal of increased brain bacterial load after CLP in our experiments. While a few mice appeared to have increased bacterial loads in the brain after CLP, it was not a consistent phenomenon across mice and did not show clear correlation with increased amyloid plaque burden. It is possible that bacteria were present in larger numbers at a different timepoint, as we only examined brains 5 days after CLP. CLP is a technique that can vary considerably

from lab to lab, so it remains feasible that we would have seen brain bacterial translocation with minor variations in our surgical technique, or if our mice had a different basal microbiome. However, our current data does not support the idea that direct bacterial translocation into the brain is the cause of the increase in plaques observed in our mice.

In summary, we report that polymicrobial sepsis in APP/PS1–21 mice is associated with a persistent neuroinflammatory response, changes in the gut microbiome, and increased hippocampal amyloid plaque deposition. These findings highlight that some of the persistent cognitive deficits seen in older sepsis survivors may be due to acceleration of amyloid plaque pathology or exacerbation of plaque-related neuroinflammation. Future experiments remain necessary to define the mechanisms underlying these pathologic findings and to assess whether sepsis affects the pathology of other neurodegenerative disease, such as Parkinson's Disease. Finally, determining whether similar changes are present in patients that have recovered from sepsis in the ICU setting is critical to ultimately translate these findings into clinically beneficial results.

Funding

This work was support in part by NIH grants T32GM108539-06 (J.M. B), R01AG054517 (E.S.M), and R01AT009741 (G.D.). A.F. received support from the Chancellor's Graduate Research Fellowship Program at Washington University in St. Louis. K.V.S. received support through the Research Scholar Award of the Society for Healthcare Epidemiology of America.

Authors' contributions

JMB and ESM conceived the study. JMB, LSC, CJN, PWS, and MFK carried out the CLP experiments, neuropathology, and data analysis. AF, KVS, and GD designed and carried out the microbiome sequencing and related data analysis. JMB, AF, and ESM wrote the manuscript, and KVS and GD provided editorial input. All authors reviewed the manuscript.

Declaration of Competing Interest

The authors declare no competing interests related to this work.

Acknowledgments

We would like to thank Dr. Richard Hotchkiss and Nemani Rateri for their help with the CLP model, as well as Dr. Carey-Ann Burnham and Meghan Wallace for assistance with microbiology.

Appendix A. Supplementary data

Supplementary data to this article can be found online at https://doi.org/10.1016/j.nbd.2021.105292.

References

Aguilar-Valles, A., Kim, J., Jung, S., Woodside, B., Luheshi, G.N., 2014. Role of brain transmigrating neutrophils in depression-like behavior during systemic infection. Mol. Psychiatry 19 (5), 599–606.
Aizenstein, H.J., Nebes, R.D., Saxton, J.A., Price, J.C., Mathis, C.A., Tsopelas, N.D., et al., 2008. Frequent amyloid deposition without significant cognitive impairment among the elderly. Arch. Neurol. 65 (11), 1509–1517.
Avramovich, Y., Amit, T., Youdim, M.B., 2002. Non-steroidal anti-inflammatory drugs stimulate secretion of non-amyloidogenic precursor protein. J. Biol. Chem. 277 (35), 31466–31473.
Banks, W.A., Gray, A.M., Erickson, M.A., Salameh, T.S., Damodarasamy, M., Sheibani, N., et al., 2015. Lipopolysaccharide-induced blood-brain barrier disruption: roles of cyclooxygenase, oxidative stress, neuroinflammation, and elements of the neurovascular unit. J. Neuroinflammation 12, 223.
Barichello, T., Fortunato, J.J., Vitali, A.M., Feier, G., Reinke, A., Moreira, J.C., et al., 2006. Oxidative variables in the rat brain after sepsis induced by cecal ligation and perforation. Crit. Care Med. 34 (3), 886–889.
Bateman, R.J., Xiong, C., Benzinger, T.L., Fagan, A.M., Goate, A., Fox, N.C., et al., 2012. Clinical and biomarker changes in dominantly inherited Alzheimer's disease. N. Engl. J. Med. 367 (9), 795–804.
Bozza, F.A., Garteiser, P., Oliveira, M.F., Doblas, S., Cranford, R., Saunders, D., et al., 2010. Sepsis-associated encephalopathy: a magnetic resonance imaging and spectroscopy study. J. Cereb. Blood Flow Metab. 30 (2), 440–448.
Brookmeyer, R., Abdalla, N., Kawas, C.H., Corrada, M.M., 2018. Forecasting the prevalence of preclinical and clinical Alzheimer's disease in the United States. Alzheimers Dement. 14 (2), 121–129.
Callahan, B.J., McMurdie, P.J., Rosen, M.J., Han, A.W., Johnson, A.J., Holmes, S.P., 2016. DADA2: high-resolution sample inference from Illumina amplicon data. Nat. Methods 13 (7), 581–583.
Caporaso, J.G., Lauber, C.L., Walters, W.A., Berg-Lyons, D., Huntley, J., Fierer, N., et al., 2012. Ultra-high-throughput microbial community analysis on the Illumina HiSeq and MiSeq platforms. ISME J. 6 (8), 1621–1624.
Davis, E.J., Foster, T.D., Thomas, W.E., 1994. Cellular forms and functions of brain microglia. Brain Res. Bull. 34 (1), 73–78.
Dodiya, H.B., Kuntz, T., Shaik, S.M., Baufeld, C., Leibowitz, J., Zhang, X., et al., 2019. Sex-specific effects of microbiome perturbations on cerebral Abeta amyloidosis and microglia phenotypes. J. Exp. Med. 216 (7), 1542–1560.
Dodiya, H.B., Frith, M., Sidebottom, A., Cao, Y., Koval, J., Chang, E., et al., 2020. Synergistic depletion of gut microbial consortia, but not individual antibiotics, reduces amyloidosis in APPPS1-21 Alzheimer's transgenic mice. Sci. Rep. 10 (1), 8183.
Dominy, S.S., Lynch, C., Ermini, F., Benedyk, M., Marczyk, A., Konradi, A., et al., 2019. Porphyromonas gingivalis in Alzheimer's disease brains: Evidence for disease causation and treatment with small-molecule inhibitors. Sci Adv. 5 (1), eaau3333.
Erickson, M.A., Banks, W.A., 2011. Cytokine and chemokine responses in serum and brain after single and repeated injections of lipopolysaccharide: multiplex quantification with path analysis. Brain Behav. Immun. 25 (8), 1637–1648.
Gasparotto, J., Girardi, C.S., Somensi, N., Ribeiro, C.T., Moreira, J.C.F., Michels, M., et al., 2018. Receptor for advanced glycation end products mediates sepsis-triggered amyloid-beta accumulation, tau phosphorylation, and cognitive impairment. J. Biol. Chem. 293 (1), 226–244.
Gofton, T.E., Young, G.B., 2012. Sepsis-associated encephalopathy. Nat. Rev. Neurol. 8 (10), 557–566.
Heneka, M.T., Carson, M.J., El Khoury, J., Landreth, G.E., Brosseron, F., Feinstein, D.L., et al., 2015. Neuroinflammation in Alzheimer's disease. Lancet Neurol. 14 (4), 388–405.
Henry, C.J., Huang, Y., Wynne, A.M., Godbout, J.P., 2009. Peripheral lipopolysaccharide (LPS) challenge promotes microglial hyperactivity in aged mice that is associated with exaggerated induction of both pro-inflammatory IL-1beta and anti-inflammatory IL-10 cytokines. Brain Behav. Immun. 23 (3), 309–317.
Hippensteel, J.A., Anderson, B.J., Orfila, J.E., McMurtry, S.A., Dietz, R.M., Su, G., et al., 2019. Circulating heparan sulfate fragments mediate septic cognitive dysfunction. J. Clin. Invest. 129 (4), 1779–1784.
Hofer, S., Bopp, C., Hoerner, C., Plaschke, K., Faden, R.M., Martin, E., et al., 2008. Injury of the blood brain barrier and up-regulation of icam-1 in polymicrobial sepsis. J. Surg. Res. 146 (2), 276–281.
Holtzman, D.M., Morris, J.C., Goate, A.M., 2011. Alzheimer's disease: the challenge of the second century. Sci Transl Med. 3 (77), 77sr1.
Hotchkiss, R.S., Moldawer, L.L., Opal, S.M., Reinhart, K., Turnbull, I.R., Vincent, J.L., 2016. Sepsis and septic shock. Nat Rev Dis Primers. 2, 16045.
Ikonomovic, M.D., Abrahamson, E.E., Isanski, B.A., Debnath, M.L., Mathis, C.A., Dekosky, S.T., et al., 2006. X-34 labeling of abnormal protein aggregates during the progression of Alzheimer's disease. Methods Enzymol. 412, 123–144.
Iwashyna, T.J., Ely, E.W., Smith, D.M., Langa, K.M., 2010. Long-term cognitive impairment and functional disability among survivors of severe sepsis. Jama. 304 (16), 1787–1794.
Iwashyna, T.J., Cooke, C.R., Wunsch, H., Kahn, J.M., 2012. Population burden of long-term survivorship after severe sepsis in older Americans. J. Am. Geriatr. Soc. 60 (6), 1070–1077.
Jack Jr., C.R., Knopman, D.S., Jagust, W.J., Shaw, L.M., Aisen, P.S., Weiner, M.W., et al., 2010. Hypothetical model of dynamic biomarkers of the Alzheimer's pathological cascade. Lancet Neurol. 9 (1), 119–128.
Jack Jr., C.R., Therneau, T.M., Weigand, S.D., Wiste, H.J., Knopman, D.S., Vemuri, P., et al., 2019. Prevalence of biologically vs clinically defined Alzheimer spectrum entities using the national institute on aging-Alzheimer's association research framework. JAMA Neurol. 76, 1174–1183.
Keren-Shaul, H., Spinrad, A., Weiner, A., Matcovitch-Natan, O., Dvir-Szternfeld, R., Ulland, T.K., et al., 2017. A unique microglia type associated with restricting development of Alzheimer's disease. Cell 169 (7) (1276-90.e17).
Knopman, D.S., Parisi, J.E., Salviati, A., Floriach-Robert, M., Boeve, B.F., Ivnik, R.J., et al., 2003. Neuropathology of cognitively normal elderly. J. Neuropathol. Exp. Neurol. 62 (11), 1087–1095.
Kumar, D.K., Choi, S.H., Washicosky, K.J., Eimer, W.A., Tucker, S., Ghofrani, J., et al., 2016. Amyloid-beta peptide protects against microbial infection in mouse and worm models of Alzheimer's disease. Sci Transl Med. 8 (340), 340ra72.
Liddelow, S.A., Guttenplan, K.A., Clarke, L.E., Bennett, F.C., Bohlen, C.J., Schirmer, L., et al., 2017. Neurotoxic reactive astrocytes are induced by activated microglia. Nature. 541 (7638), 481–487.
Martin, G.S., Mannino, D.M., Moss, M., 2006. The effect of age on the development and outcome of adult sepsis. Crit. Care Med. 34 (1), 15–21.
McMurdie, P.J., Holmes, S., 2013. phyloseq: an R package for reproducible interactive analysis and graphics of microbiome census data. PLoS One 8 (4), e61217.

Michels, M., Vieira, A.S., Vuolo, F., Zapelini, H.G., Mendonca, B., Mina, F., et al., 2015. The role of microglia activation in the development of sepsis-induced long-term cognitive impairment. Brain Behav. Immun. 43, 54–59.
Minter, M.R., Zhang, C., Leone, V., Ringus, D.L., Zhang, X., Oyler-Castrillo, P., et al., 2016. Antibiotic-induced perturbations in gut microbial diversity influences neuro-inflammation and amyloidosis in a murine model of Alzheimer's disease. Sci. Rep. 6, 30028.
Minter, M.R., Hinterleitner, R., Meisel, M., Zhang, C., Leone, V., Zhang, X., et al., 2017. Antibiotic-induced perturbations in microbial diversity during post-natal development alters amyloid pathology in an aged APPSWE/PS1DeltaE9 murine model of Alzheimer's disease. Sci. Rep. 7 (1), 10411.
Pandharipande, P.P., Girard, T.D., Jackson, J.C., Morandi, A., Thompson, J.L., Pun, B.T., et al., 2013. Long-term cognitive impairment after critical illness. N. Engl. J. Med. 369 (14), 1306–1316.
Peskind, E.R., Li, G., Shofer, J., Quinn, J.F., Kaye, J.A., Clark, C.M., et al., 2006. Age and apolipoprotein E*4 allele effects on cerebrospinal fluid beta-amyloid 42 in adults with normal cognition. Arch. Neurol. 63 (7), 936–939.
Quast, C., Pruesse, E., Yilmaz, P., Gerken, J., Schweer, T., Yarza, P., et al., 2013. The SILVA ribosomal RNA gene database project: improved data processing and web-based tools. Nucleic Acids Res. 41 (Database issue), D590–D596.
Radde, R., Bolmont, T., Kaeser, S.A., Coomaraswamy, J., Lindau, D., Stoltze, L., et al., 2006. Abeta42-driven cerebral amyloidosis in transgenic mice reveals early and robust pathology. EMBO Rep. 7 (9), 940–946.
Sastre, M., Dewachter, I., Landreth, G.E., Willson, T.M., Klockgether, T., van Leuven, F., et al., 2003. Nonsteroidal anti-inflammatory drugs and peroxisome proliferator-activated receptor-gamma agonists modulate immunostimulated processing of amyloid precursor protein through regulation of beta-secretase. J. Neurosci. 23 (30), 9796–9804.
Segata, N., Izard, J., Waldron, L., Gevers, D., Miropolsky, L., Garrett, W.S., et al., 2011. Metagenomic biomarker discovery and explanation. Genome Biol. 12 (6), R60.
Selkoe, D.J., Hardy, J., 2016. The amyloid hypothesis of Alzheimer's disease at 25 years. EMBO Mol Med. 8 (6), 595–608.
Semmler, A., Frisch, C., Debeir, T., Ramanathan, M., Okulla, T., Klockgether, T., et al., 2007. Long-term cognitive impairment, neuronal loss and reduced cortical cholinergic innervation after recovery from sepsis in a rodent model. Exp. Neurol. 204 (2), 733–740.
Semmler, A., Hermann, S., Mormann, F., Weberpals, M., Paxian, S.A., Okulla, T., et al., 2008. Sepsis causes neuroinflammation and concomitant decrease of cerebral metabolism. J. Neuroinflammation 5, 38.
Semmler, A., Widmann, C.N., Okulla, T., Urbach, H., Kaiser, M., Widman, G., et al., 2013. Persistent cognitive impairment, hippocampal atrophy and EEG changes in sepsis survivors. J. Neurol. Neurosurg. Psychiatry 84 (1), 62–69.
Shin, N.R., Whon, T.W., Bae, J.W., 2015. Proteobacteria: microbial signature of dysbiosis in gut microbiota. Trends Biotechnol. 33 (9), 496–503.
Singer, B.H., Newstead, M.W., Zeng, X., Cooke, C.L., Thompson, R.C., Singer, K., et al., 2016. Cecal ligation and puncture results in long-term central nervous system myeloid inflammation. PLoS One 11 (2), e0149136.
Singer, B.H., Dickson, R.P., Denstaedt, S.J., Newstead, M.W., Kim, K., Falkowski, N.R., et al., 2018. Bacterial dissemination to the brain in Sepsis. Am. J. Respir. Crit. Care Med. 197 (6), 747–756.
Skelly, D.T., Hennessy, E., Dansereau, M.A., Cunningham, C., 2013. A systematic analysis of the peripheral and CNS effects of systemic LPS, IL-1beta, [corrected] TNF-alpha and IL-6 challenges in C57BL/6 mice. PLoS One 8 (7), e69123.
Sonneville, R., Verdonk, F., Rauturier, C., Klein, I.F., Wolff, M., Annane, D., et al., 2013. Understanding brain dysfunction in sepsis. Ann. Intensive Care 3 (1), 15.
Soscia, S.J., Kirby, J.E., Washicosky, K.J., Tucker, S.M., Ingelsson, M., Hyman, B., et al., 2010. The Alzheimer's disease-associated amyloid beta-protein is an antimicrobial peptide. PLoS One 5 (3), e9505.
Tejera, D., Mercan, D., Sanchez-Caro, J.M., Hanan, M., Greenberg, D., Soreq, H., et al., 2019. Systemic inflammation impairs microglial Abeta clearance through NLRP3 inflammasome. EMBO J. 38 (17), e101064.
Unsinger, J., McGlynn, M., Kasten, K.R., Hoekzema, A.S., Watanabe, E., Muenzer, J.T., et al., 2010. IL-7 promotes T cell viability, trafficking, and functionality and improves survival in sepsis. J. Immunol. 184 (7), 3768–3779.
Villemagne, V.L., Burnham, S., Bourgeat, P., Brown, B., Ellis, K.A., Salvado, O., et al., 2013. Amyloid beta deposition, neurodegeneration, and cognitive decline in sporadic Alzheimer's disease: a prospective cohort study. Lancet Neurol. 12 (4), 357–367.
Wang, X., Sun, G., Feng, T., Zhang, J., Huang, X., Wang, T., et al., 2019. Sodium oligomannate therapeutically remodels gut microbiota and suppresses gut bacterial amino acids-shaped neuroinflammation to inhibit Alzheimer's disease progression. Cell Res. 29 (10), 787–803.
Wendeln, A.C., Degenhardt, K., Kaurani, L., Gertig, M., Ulas, T., Jain, G., et al., 2018. Innate immune memory in the brain shapes neurological disease hallmarks. Nature. 556 (7701), 332–338.
Widmann, C.N., Heneka, M.T., 2014. Long-term cerebral consequences of sepsis. Lancet Neurol. 13 (6), 630–636.
Wright, E.S., 2015. DECIPHER: harnessing local sequence context to improve protein multiple sequence alignment. BMC Bioinforma. 16, 322.
Yamamoto, M., Kiyota, T., Horiba, M., Buescher, J.L., Walsh, S.M., Gendelman, H.E., et al., 2007. Interferon-gamma and tumor necrosis factor-alpha regulate amyloid-beta plaque deposition and beta-secretase expression in Swedish mutant APP transgenic mice. Am. J. Pathol. 170 (2), 680–692.
Zaghloul, N., Addorisio, M.E., Silverman, H.A., Patel, H.L., Valdes-Ferrer, S.I., Ayasolla, K.R., et al., 2017. Forebrain cholinergic dysfunction and systemic and brain inflammation in murine Sepsis survivors. Front. Immunol. 8, 1673.
Zhao, J., Bi, W., Xiao, S., Lan, X., Cheng, X., Zhang, J., et al., 2019. Neuroinflammation induced by lipopolysaccharide causes cognitive impairment in mice. Sci. Rep. 9 (1), 5790.
Zhou, Y., Song, W.M., Andhey, P.S., Swain, A., Levy, T., Miller, K.R., et al., 2020. Human and mouse single-nucleus transcriptomics reveal TREM2-dependent and TREM2-independent cellular responses in Alzheimer's disease. Nat. Med. 26 (1), 131–142.